A Monte Carlo Study of Host-Material Deformation Effect on Li Migration in Graphite

Ryo Kobayashi,[1]* Nobuko Ohba,[2] Tomoyuki Tamura,[3] and Shuji Ogata[1]

[1]*Department of Scientific and Engineering Simulation, Nagoya Institute of Technology,*

Gokiso-cho, Showa-ku, Nagoya 466-8555, Japan

[2]*Toyota Centeral Research & Development Laboratories, Inc., Nagakute, Aichi 480-1192,*

Japan

[3]*Center for Fostering Young and Innovative Researchers, Nagoya Institute of Technology,*

Gokiso-cho, Showa-ku, Nagoya 466-8555, Japan

Monte Carlo simulation has been performed to investigate the variation of chemical diffusion coefficient of Li ions in graphite as a function of applied voltage and its relation to the staging phenomenon. The interatomic potential between Li ions is parametrized using density functional theory and molecular statics to include interactions between Li ions through host-material elastic deformation. The present simulation in a bulk graphite system can simulate Li ion migration without uncertainties encountered in some experiments, and well reproduces not only $\sqrt{3} \times \sqrt{3}$ in-plane super lattice and stage structures observed in experiments, but also the decrease of chemical diffusion coefficient when two phases coexist reflecting the drop of thermodynamic factor. We have clearly shown that the stage structure and decrease of the chemical diffusion coefficient can be explained with only the interaction between Li ions through the deformation of host material. Furthermore we have found substages between stage-1 and -2 which may cause further uncertainties for the observation of the diffusion coefficient in the experiments.

KEYWORDS: Monte-Carlo simulation; Lithium-ion diffusion

1. Introduction

Some classes of Li ion batteries are widely used and play key roles in various mobile devices. For future electric devices and electric vehicles, it is required for the Li ion batteries to have more capacity and faster charge-discharge capability. In the Li ion batteries, Li ions migrate from a negative electrode to a positive electrode through electrolyte during discharg-

∗E-mail: kobayashi.ryo@nitech.ac.jp

ing, and migrate in the reverse direction during charging. It is necessary to understand Li ion

migrations in the negative and positive electrodes, electrolyte, and their interfaces to achieve

remarkable improvement required in the industrial field. However, there are a lot of things

remaining that we have to understand more even in a bulk electrode.

Li ion migration in the negative electrode is a characteristic example; the negative elec-

trode made of graphite stores Li ions in its inter-layer spaces and Li ions migrate in two

dimensional sites in a layer. Although this Li ion migration phenomenon is simple, the dif-

fusion coefficients reported by many researchers widely diverge in a range of 10^{-6} to 10^{-12}

cm^2/s.[1–5]

This divergence is considered to be caused by the dependence of the coefficient on ap-

plied voltage. It is well known that Li ions form $\sqrt{3} \times \sqrt{3}$ super lattice structure within a basal

plane of graphite and show several stage structures depending on applied voltage.[6–8] And it is

also known that the diffusion coefficient is dependent on the stage structure and it decreases

significantly when the stage structure changes. This decrease is believed to be the result of

drop of thermodynamic factor or redox capacitance. Usually the diffusion coefficient is ob-

tained using potentiostatic or galvanostatic intermittent titration technique (PITT or GITT),

or electrochemical impedance spectroscopy (EIS).[1–5,9] And uncertainties in measurements of

Li ion density, geometric edge plane area, and redox capacitance also seem to cause a huge

error of diffusion coefficient values reported.

There are some theoretical research to study Li ion migration of ideal situation in a bulk

graphite avoiding the uncertainties in the experiments. Toyoura *et al.* investigated the diffu-

sion coefficient in case of high density around LiC_6 by means of density functional theory (DFT) calculations.[10,11] They showed that the diffusivity drastically changes between Li ion deficiency and excess from the density around LiC_6. Persson *et al.* also calculated the diffusion coefficient at high density close to LiC_6[12,13] using DFT and kinetic Monte Carlo (KMC) simulations and concluded that the Li ion diffusion coefficient decreases as the density increases between Li density of stage-2 and -1. However, as suggested by Safran and Hamann,[6] it seems that the interaction between Li ions through the elastic deformation of host material plays a key role for the formation of the stage structures. And the recent hybrid quantum-mechanics and classical mechanics (QM-CL) study showed that an intercalated Li ion pushes and spreads out graphite layers making cage-like structure around it, and Li ion diffusivity is affected by the pressure normal to graphite layers.[14,15] These preceding studies suggest that we need to take into account the effects of host-material deformation for the calculation of Li diffusion coefficient. The studies based on DFT cannot treat the long-range interaction between Li ions through host-material deformation, because DFT requires high computational cost and it is hard to apply DFT to the system large enough to take the elastic deformation into consideration.

Molecular dynamics (MD) simulation with classical interatomic potentials is a good candidate which enables us to consider the effect through host-material deformation. Márguez and Balbuena performed MD simulation of Li intercalation at the interface of graphite and electrolyte using a variable-charge interatomic potential,[16] and concluded that repulsive Coulombic interactions between Li ions determines staging phenomena. However, as far as

we know, no research using MD reproduce the stage structures in graphite. And, since the migrations of Li ions are rare events in some cases, very long computation time may be required to obtain enough statistical data to evaluate the diffusion coefficient in MD.

Monte Carlo (MC) methods are event-driven methods which allow us to simulate very long-time (rare event) phenomena. Thus, in this paper, to clarify the origin of the variation of chemical diffusion coefficient as a function of applied voltage, we adopt MC methods (standard MC, KMC, and grand canonical MC (GCMC)) with a simple effective potential between Li ions which explicitly includes the contribution from the host-material deformation. The potential and determination of the parameters in the potential are described in Secs. 2.2 and 2.3. We use standard MC to investigate equilibrium Li structures under various conditions (Sec. 3.1), KMC for calculating the diffusion coefficient (Sec. 3.2), and GCMC for investigating the variation of the coefficient as a function of applied voltage (Sec. 3.3).

2. Calculation Method

2.1 Li migration model in graphite

In order to model the Li migration in graphite, we do not treat explicitly C atoms that construct the host graphite. Instead, we assume an effective potential between Li ions which incorporates the interaction coming from host-material elastic deformation. And a Li ion is assumed to hop from a site to the other sites under the effective potential. Avoiding to treat explicitly C atoms and simplifying the Li migration in such a way, we can simulate the Li migration very efficiently compared to the case that we treat all the motions of atoms including C atoms.

It is known that, when there are no intercalated Li ions, graphite forms AB-stacking in which a half of C atoms in neighboring layers are placed at the superposing position along the stacking direction. If there are a certain amount of Li ions intercalated into graphite, graphite forms AA-stacking in which all the C atoms in neighboring layer are at the superposing position. Since, in this paper, we are interested in the relation between the stage structures and diffusivity of Li ions, we focus only on the AA-stacking. Note that we apply this model also to very low Li density, because it is worth studying the density dependence of Li diffusivity in whole range of Li density. The results obtained in this paper for low Li density are not comparable to the experimental ones.

In AA-stacking, the sites to be occupied by Li ions form a triangle lattice. Li ions can migrate to their first nearest neighbor sites only in the same layer in this model, since the energy barrier for migration to neighbouring layer is an order of magnitude higher than that of in-plane migration.

2.2 *On-site potential energy and transition-state energy*

Since we focus on the contribution of the host-material deformation to Li diffusivity, we consider an effective potential between Li ions which consists of explicit contributions of host-material deformation and electrostatic parts. In order to perform standard MC simulation, we firstly define the on-site (OS) potential energy of a site-i as

$$V_{\mathrm{OS}}(i) \equiv \sum_{j \in L_0, \mathrm{n.n.}} \phi^{\mathrm{R}}_{\mathrm{Coulomb}}(i, j) + V_{\mathrm{deform}}(i) \tag{1}$$

with

$$V_{\text{deform}}(i) = \sum_{j \in L_0} \phi_{\text{deform}}^{\text{A}}(i, j) + \sum_{j \notin L_0} \phi_{\text{deform}}^{\text{R}}(i, j) \tag{2}$$

where L_0 means the layer where the site-i exists. The first term on the right hand side of Eq. (1) means that the repulsive Coulombic interactions work only within Li ions at the first nearest neighbor (n.n.) sites on the same layer. The contribution of host-material deformation, $V_{\text{deform}}(i)$, consists of attractive interactions between Li ions on the same layer (the first term on the right hand side of Eq. (2)), and repulsive interactions between Li ions on different layers (the second term), which will be parametrized through the molecular static simulation as described in Sec. 2.3. Note that we assume the repulsive Coulombic interaction decays within very short distance and does not work for Li ions further than the second nearest neighbor sites because of the screening effect from electrons around the C atoms. Although it is too simplified and the Coulomb interaction in a real situation may reach further distance, we are not able to estimate accurate Coulomb interaction because we do not know how much it is screened. Besides, this simplification helps us to extract only the effect of host-material deformation between Li ions. On the other hand, we neglect the screening effect of the elastic field in the case that more than two Li ions exist in the interaction range. From the above reasons, since we can not evaluate the diffusion coefficient of Li ion quantitatively with this model, we will discuss the qualitative change of Li diffusivity as a function of Li density caused by the the interactions between Li ions through host-material deformation.

To perform KMC simulation, we need to calculate the probability of occurrence of every event, that is, we need the activation energy of Li migration. The evaluation of this quantity

is a crucial factor in the study of diffusion. We define the activation energy which is required

to escape from a site-i as

$$E_a(i) \equiv V_{TS}(i) - V_{OS}(i), \tag{3}$$

with the transition-state (TS) energy defined as

$$V_{TS}(i) \equiv E_a^0 + \lambda V_{deform}(i) \tag{4}$$

where the reference activation energy, E_a^0, which is the activation energy of an isolated Li

ion in the frozen or fixed host graphite, is determined from DFT calculation of Li migration

without any elastic deformation at 0 K. Note that, although the activation energy should be

dependent on each migration direction (six nearest neighbor directions) in real system, we

neglect such a dependency and set an identical value to each direction. Although the TS

energy would be also influenced by contribution of the host-material deformation through

host-material deformation, it is not easy to evaluate the contributions quantitatively. Here, in

this model, we assume that the contributions to the TS energy is multiple of that to the OS

energy. In the case of $\lambda = 1$ in Eq. (4), the contributions in the OS energy and TS energy

compensate each other and all the energy barriers are equal except those include repulsive

Coulombic effects. In the case of $\lambda > 1$, the contributions in the TS energy exceed those in

the OS energy. This is counter-intuitive because the transition rate from low-energy state to

higher-energy state is higher than that of reverse direction, and the system goes to an unstable

configuration. Consequently, λ should be smaller than 1 to reproduce the stage structures

observed in experiments.

2.3 Parametrization of effective potential

It is necessary to make a parameter table of the OS potential energy in Eq. (1) between two Li ions on sites i and j. These potential parameters were obtained by a bottom-up approach through the following procedure.

Firstly, the potential energy of Li ion as a function of z position in an inter-layer spacing of graphite (assuming the graphite layer lies on xy plane) was calculated using DFT. For this calculation, the Tokyo *ab-initio* program package (TAPP) was used.[17] In the DFT calculation, wave functions were expanded with plane waves up to the energy cutoff 500 eV. The generalized gradient approximation[18] (GGA) was used for the exchange-correlation potential and the ultrasoft pseudopotential was adopted for Li and C atoms. It is known that GGA does not reproduce accurate inter-layer distance of graphite, and we have to take the van der Waals (vdW) interaction into account to achieve this. However, since we only require Li-C interaction in a layer in which an electro-chemical interaction dominates rather than the vdW interaction, here we used GGA and did not consider the vdW interaction (vdW interactions were taken into account in the molecular statics calculations described below.) There were 12 C and one Li atoms in a supercell which had two atomic layers of inter-layer distance, 3.7 Å, and C atoms form AA-stacking and they are fixed to their original positions. The energy differences between the system with one Li and 12 C atoms and the system with only 12 C atoms as a function of z position of Li atom are plotted in Fig. 1.

Secondly, we assumed the repulsive potential function between Li and C atoms as

$$\varphi_{\text{Li-C}}(r) \quad = \quad \varphi_0 + \epsilon \left(\frac{\sigma}{r} \right)^n + \epsilon \left(\frac{\sigma}{r_c} \right)^n$$
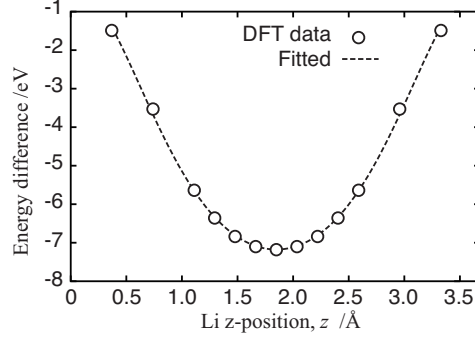
Fig. 1. Energy difference as a function of z position of Li atom obtained by DFT calculation (circles) and the fitted function $\varphi_{\mathrm{Li-C}}$ (dotted line).

Table I. Potential parameters obtained by fitting the function $\varphi_{\mathrm{Li-C}}$ to the DFT data.

n	2	
r_{c}	2.35	Å
σ	2.12	Å
ϵ	1.53	eV
φ_0	-7.23	eV

$$-(r - r_{\mathrm{c}})\left[-n\epsilon\left(\frac{\sigma}{r_{\mathrm{c}}}\right)^{n}\frac{1}{r_{\mathrm{c}}}\right],\tag{5}$$

where r and r_{c} are distance between Li and C atoms and cutoff radius, respectively. Fitting the parameters ϵ, σ, and n of the function with the DFT data set obtained by the above procedure, we obtained the interatomic potential for Li-C interaction (Table I). Note that this Li-C interatomic potential works only on this purpose and cannot reproduce activation energy of Li-ion migration.

Finally, using Brenner potential[19] for C-C interaction, Ohba potential[15] for the inter-layer vdW interaction, and the potential for Li-C interaction obtained above, we performed molec-

Table II. The parameter table of the deformation effect of potential energy $\phi_{\mathrm{deform}}(i, j)$ in meV.

	0th n.n.	1st n.n.	2nd n.n.
0th layer	—	-68	-35
1st layer	+77	+52	+4
2nd layer	+27	+14	+3
3rd layer	+13	+10	+5

ular statics (MS) simulation to obtain the parameter table of strain energy term in Eq. (2). The

system of MS simulation was a periodic crystalline AA-stacking graphite of the size larger

than 25 Å in x and y directions and more than 30 layers of interlayer distance 3.7 Å in z

direction, which was large enough to neglect the effects from periodic images. We computed

the difference of total potential energies between relaxed and non-relaxed structures includ-

ing two Li ions at sites i and j, $\Delta E(i, j)$, and then obtained the Li-Li interaction potential

$\phi_{\mathrm{deform}}(i, j)$ as

$$\phi_{\mathrm{deform}}(i, j) = \Delta E(i, j) - 2\Delta E(i), \tag{6}$$

where $\Delta E(i)$ is the energy difference between relaxed and non-relaxed structures including

only one Li ion at site-i. Note that the relaxation took place only in z direction to keep

AA-stacking. Table II shows calculated Li-Li interaction potential $\phi_{\mathrm{deform}}(i, j)$ through host-

material deformation and we can see that the deformation effect is attractive in the case that

two Li ions are on the same layer and repulsive otherwise.

2.4 Monte Carlo simulation algorithm

Standard, kinetic, and grand-canonical MC methods with the effective potential described above are adopted in this paper. Li ions move on triangular lattice sites which represent Li stable sites in AA-stacking graphite.

In the standard MC method, firstly we move a randomly chosen Li ion to a neighboring site which is chosen randomly from six first nearest neighbor sites. Compute the potential energy of the new configuration, E^{new}. Comparing it with the energy of the old configuration, E^{old}, we accept the new configuration with the probability,

$$\min\left[1, \ \exp\left(-\frac{E^{\text{new}} - E^{\text{old}}}{k_{\text{B}}T}\right)\right]. \tag{7}$$

where T and k_{B} are temperature of the system and Boltzmann factor. In case of the GCMC method, the event of particle addition or deletion takes place at every 10 MC steps with probabilities,

$$\min\left[1, \frac{V}{\Lambda^3(N+1)} \exp\left\{\frac{\mu - E(N+1) + E(N)}{k_{\text{B}}T}\right\}\right] \tag{8}$$

or

$$\min\left[1, \frac{\Lambda^3(N)}{V} \exp\left\{-\frac{\mu + E(N-1) - E(N)}{k_{\text{B}}T}\right\}\right], \tag{9}$$

respectively. Here $E(N)$ is the potential energy of N-ion system, V is the volume of the system, and $\Lambda \equiv h/\sqrt{2\pi m_{\text{Li}}k_{\text{B}}T}$ is the thermal de Broglie wavelength of Li ion, where m_{Li} is the mass of Li ion. The chemical potential, μ, corresponds to the applied voltage in Fig. 7.

In the kinetic MC method, we calculate the energy barrier, $E_{\text{a}}(i)$ (in Eq. (3)), and transition probability, $\Gamma_{i \rightarrow j} = \nu \exp(-E_{\text{a}}(i)/k_{\text{B}}T)$, of every process (Li on site-i moves to neighboring

site-j) where v is a trial frequency of the Li ion. Parameters are set to the values in Table III

during simulation runs. A process is chosen from the list of event using a random number.

And the time interval by which the event takes place is also computed using these probabilities

and a random number, r, as $\Delta t = -\ln(r)/\Gamma$ where $\Gamma = \sum_{i,j} \Gamma_{i \to j}$.

2.5 *Calculation of diffusion coefficients*

The flux of a chemical species is proportional not to the density gradient but to the chem-

ical potential gradient of the species. Its coefficient D_C, which is called chemical diffusion

coefficient, obtained in some experiments such as PITT and EIS has to do with the jump

diffusion coefficient D_J which connects the flux and density gradient as[20–23]

$$D_C = \Theta D_J \tag{10}$$

where

$$D_J = \lim_{t \to \infty} \frac{1}{2dt} \left\langle \frac{1}{N} \left(\sum_i^N \Delta \boldsymbol{r}_i(t) \right)^2 \right\rangle. \tag{11}$$

Here d is the dimension of diffusing space, which is two in the case of graphite intercalation

compounds, $\Delta \boldsymbol{r}(t)$ is the displacement of time t from the initial position, N is the number of

Li ions in the system. And Θ is the thermodynamic factor,

$$\Theta = \left(\frac{\partial(\mu/k_B T)}{\partial \ln\langle N \rangle} \right) = \frac{\langle N \rangle}{\langle \delta N^2 \rangle}, \tag{12}$$

where $\langle \cdots \rangle$ means the ensemble average and $\langle \delta N^2 \rangle \equiv \langle N^2 \rangle - \langle N \rangle^2$. The second equality in

Eq. (12) is used to calculate Θ in GCMC simulation. This relation may not be applicable to

an inhomogeneous system such that two phases coexist. Hence we should be careful when

we discuss about the quantitative analysis of Θ at the phase transition points. We compute

tracer (self) diffusion coefficient

$$D^* = \lim_{t \to \infty} \frac{1}{2dt} \frac{1}{N} \sum_i^N \left\langle (\Delta \boldsymbol{r}_i(t))^2 \right\rangle \tag{13}$$

instead of D_J. The difference between D^* and D_J is that whether there are cross terms of species $i \neq j$. We neglect the cross terms in this paper because they don't have significant dependency on the Li ion density compared to the thermodynamic factor.[22]

3. Results and Discussion

3.1 Intralayer and staging structures with respect to the OS energy

To clarify the effect of host-material deformation on the formation of Li structures, we performed standard MC simulation runs of several cases with or without contributions from host-material deformation. The simulation system was prepared by periodically copying the unit cell which includes two Li sites, and we will denote the number of copies in each direction as (n_x, n_y, n_z) hereafter. In the case of the simulation without inter-layer potentials (the second term of the right hand side of Eq. (2)), we used the system made of $(n_x, n_y, n_z) = (80, 42, 1)$ cells which included 6720 Li sites and periodic along the layer (xy-plane) and not perpendicular to the layer. In the case with inter-layer potentials, the system was of size $(42, 20, 6)$ which had 6 layers and 1680 Li sites in a layer and periodic to all directions. The parameters used in these simulation runs are listed in Table III and all the simulation was performed at room temperature. The repulsive Coulombic potential value was determined to reproduce the reduction of activation energy of an interstitial Li ion in $\sqrt{3} \times \sqrt{3}$ super lattice reported by Toyoura et al.[11] We adopted the trial frequency value, ν, as

Table III.   Parameters used in MC simulation runs.

E_a^0	0.45	eV
$\phi_{Coulomb}^R$	0.1	eV
T	300	K
ν	1.0×10^{13}	s^{-1}

Table IV.   The cases of interaction variations considered in this paper. The symbols —, ○, and △ indicate that the interaction is not included, included, and included only between nearest neighbour sites, respectively.

	Coulomb	Deformation effect	
		Intra-layer	Inter-layer
Case-0	—	—	—
Case-1	○	—	—
Case-2	○	△	—
Case-3	○	○	—
Case-4	○	○	○

shown in Table III which is commonly used for this system.[12, 13]

Firstly, we investigated the Li structure in the case of no OS potential (case-0 as shown in Table IV). Since there is only exclusive interaction between Li ions, no regular structure of Li ions appears even at high Li density as shown in Fig. 2.

Next, we considered only the repulsive interaction between nearest neighbor sites (case-1), namely only the first term on the right hand side in Eq. (1). Since Li ions at nearest neighbor sites repel each other, Li ions tend to form $\sqrt{3} \times \sqrt{3}$ super lattice structure when Li density is as high as x in Li$_x$C$_6$ close to 1.0.
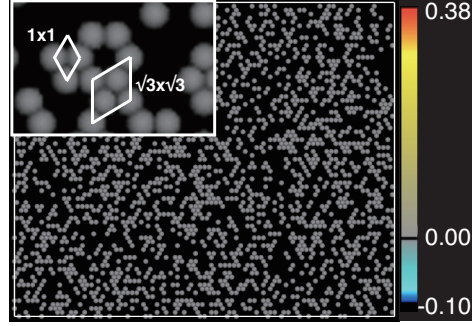
Fig. 2. (Color) Li structure in a layer in the case of $x = 1.0$ in Li_xC_6 without Li-Li interactions. The color of an ion means on-site potential energy in eV and all the ions have 0 values because there are no interactions. The inset shows 1×1 and $\sqrt{3} \times \sqrt{3}$ unit cells of Li ions. No C atom is shown since we do not consider C atoms explicitly in the present simulation. It is clear that no regular structure of Li appears in this case.
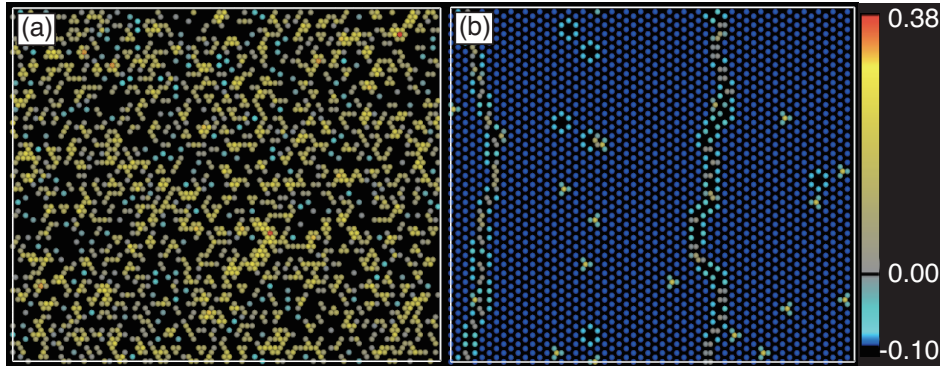
Fig. 3. (Color) Li structures of LiC_6 in case-3: (a)initial configuration and (b)the structure after equilibration in which we can see $\sqrt{3} \times \sqrt{3}$ structure. Ions are colored according to their on-site potential energy in eV.

In the case that the deformation effect with only nearest neighbors in the same layer was taken into account (case-2), the repulsive energy between nearest neighbors became weak from 0.1 to 0.032 eV. And $\sqrt{3} \times \sqrt{3}$ super lattice was also formed when the Li density is high.

In the case that we take into account all the interactions in the same layer (case-3), namely
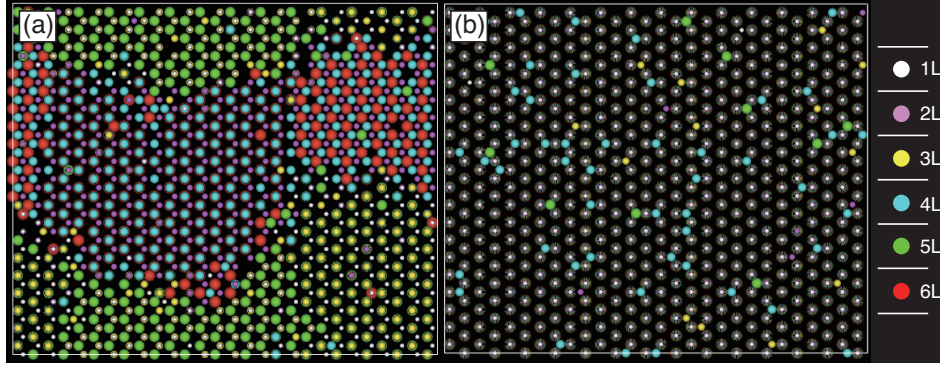
Fig. 4. (Color) Li structures in case-4. (a)In the case of Li density $x = 0.5$, Li ions form stage-2 structure, and (b)in the case of Li density $x = 1.0$, Li ions form stage-1 structure. The colors of ions indicate the layer to which the ions belong.

using the first term in the right hand side of Eq. (1) and the first term in right hand side of Eq. (2), attractive interactions work between Li ions further than the first nearest neighbor sites. Because of these attractive interactions, Li ions formed $\sqrt{3} \times \sqrt{3}$ super lattice as shown in Fig. 3(b), and those Li ions had low potential energies (blue-color circles in Fig. 3(b)). And this $\sqrt{3} \times \sqrt{3}$ structure was formed even at low Li density unlike above two cases, case-1 and -2. We can see that the formation of in-plane $\sqrt{3} \times \sqrt{3}$ super lattice structure is attributed to the balance between repulsive Coulombic interaction and attractive interaction through host-material deformation in the same layers.

When we took into account all the interactions including inter-layer ones, the stage-2 and -1 structures were observed at the densities $x = 0.5$ and 1.0, respectively, as shown in Fig. 4. The structures of longer period than stage-3 were not observed in this system at room temperature. In the stage-1 structure, Li ions took the same $\sqrt{3} \times \sqrt{3}$ commensurate sites along z direction. However, Li ions took the incommensurate sites between layers at room

temperature in the stage-2 structure. The present model well reproduces the Li structures such as $\sqrt{3} \times \sqrt{3}$ super lattice and staging depending on the Li density. And from these results, it is clear that the effect of host-material deformation between Li ions of different layers plays a key role for the staging phenomena as suggested by Safran and Hamann,[6] which is a different conclusion from Márguez and Balbuena.[16]

3.2 D^* as a function of Li density

We performed KMC simulation to investigate the dependence of the tracer diffusion coefficient on Li density. In the KMC simulation, we calculated transition rates from one site to another using Eqs. (1)–(4). Figure 5 shows the tracer diffusion coefficients of all the cases described in the previous section and shown in Table IV as a function of Li density (x in Li_xC_6). Note that the assumption, which Li ions migrate in an AA-stacking structure, does not hold for dilute Li concentration in real systems because graphite has an AB-stacking structure in a dilute case. However it is worth studying even for a dilute case with this assumption to understand the variation of the diffusion coefficient as a function of Li density.

Li ion diffusivity is strongly dependent on the interatomic potential used. In the case-0, as the density increases, the rate of collision between Li ions increases and they block each other, consequently the diffusivity decreases. In the case-1 and -2, if two Li ions collide with each other, they feel repulsion and migrate very fast. Thus the diffusivity rises as a function of the density. Especially, in the case-1, the diffusivity jumps orders of magnitude around the density $x \sim 1.0$, because of the very strong repulsion. In the case-3, which the repulsive Coulombic interaction and attractive deformation effects between Li ions only on the same
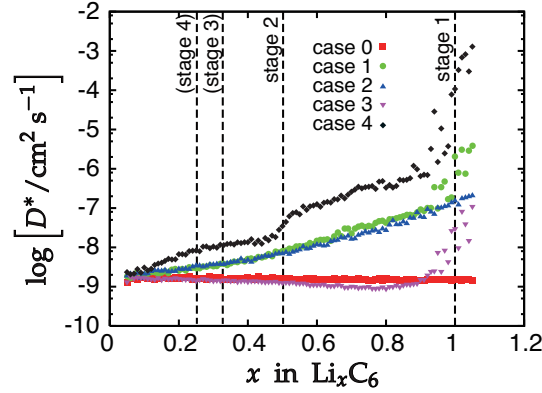
Fig. 5. (Color online) The tracer diffusion coefficient as a function of the Li-density in several cases of Li-Li interactions.

layer are considered, interestingly, the diffusivity decreases as a function of the density until the density, x, becomes higher than about 0.8. This is because the attractive effect of host-material deformation reaches further than the repulsive one and Li ions further than the first nearest neighbor sites are weekly trapped by this attractive potential. And since the OS potential energy of the first nearest neighbors is as same as the case-2, the diffusivity at the density over 1.0 rises to the same value as the case-2. In the case-4, which interactions between layers are taken into account, the diffusivity also increases monotonically as a function of the density. However, unlike the other cases, the diffusivity curve has a shoulder at the density $x \sim 0.5$. This reflects the situation that Li ions caught between layers that are fully filled with Li ions feel as if they are in a small and uncomfortable room when the density, x, is higher than 0.5.

The dependency of the diffusivity on λ in Eq. (4) was also studied in the case-4. Figure 6 shows the tracer diffusion coefficients as a function of Li density in cases of $\lambda = 0.5, 0.0,$
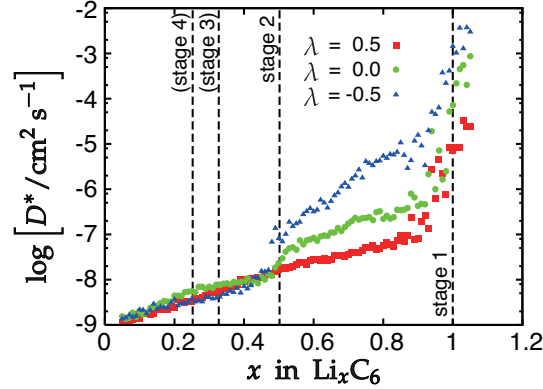
Fig. 6. (Color online) The tracer diffusion coefficient as a function of the Li-density in several cases of λ values.

and -0.5. As described previously, λ should be less than 1.0. And if so, the λ value does not change qualitatively the transition rate relation that Li ions tend to go from unstable sites to stable sites, but changes the degree of the barrier height. Therefore the variation of λ in the range $\lambda < 1.0$ only shifts the diffusion coefficient at high density region, $x > 0.5$.

3.3 Θ and D_C as a function of applied voltage

To investigate the variation of staging and diffusion coefficient as a function of applied voltage, we performed GCMC simulation with respect to a variety of chemical potentials of external particle source. Full deformation effects including the inter-layer interaction and $\lambda = 0$ in Eq. (4) for the TS energy were adopted. The simulation system was made of (24,12,6) cells which included 3456 Li sites in total with periodicity along all directions. The chemical potential was controlled so that the applied voltage of the system gradually decreases, which corresponds to charging of Li ion batteries. On each applied voltage, after the equilibration by GCMC, the average number of Li ions in the system, $\langle N \rangle$, was computed and the diffusion

coefficient was calculated by KMC with that configuration.

Figure 7(a) shows the average number of Li ions in the system as a function of the applied voltage, E. This clearly shows the staging phenomenon of Li intercalation compounds; stage-3 ($\langle N \rangle \sim 384$) around $E = 0.4$ V, stage-2 ($\langle N \rangle \sim 576$) from 0.2 V to 0.38 V, and stage-1 ($\langle N \rangle \sim 1152$) under 0.07 V. Interestingly, there are two phases observed between stage-2 and stage-1 around $E \sim 0.15$ V ($\langle N \rangle \sim 768$) and $E \sim 0.1$ V ($\langle N \rangle \sim 960$), in which one and two of the three empty layers in stage-2 are filled, respectively. Note that, since the deformation effects in the present potential neglect screening effects as described previously, the present potential overestimates deformation effects in the case of high density situation. Therefore those substages appear in somewhat wide range of applied voltage in this simulation. If the screening effects are taken into account, this range would be smaller and it may be difficult to identify those substages in experiments.

The thermodynamics factor, Θ, computed using Eq. (12) is shown in Fig. 7(b) as a function of the applied voltage. The Θ has large values (over 1,000) when a stage structure is stable. On the other hand, it drops drastically at the voltage that the two stage structures co-exist. The Θ values obtained at these phase transition points are unreliable and should be zero from its definition (hence we show downward arrows at these points in Fig. 7). However computed Θ corresponds to the inverse of a redox capacitance measured in EIS experiments,[2,3] and thus it is worth discussing about the drops of Θ at these points. As a consequence, the chemical diffusion coefficient, D_C, also drops at these points even though the tracer diffusion coefficient, D^*, monotonically decreases as a function of the applied voltage as seen in
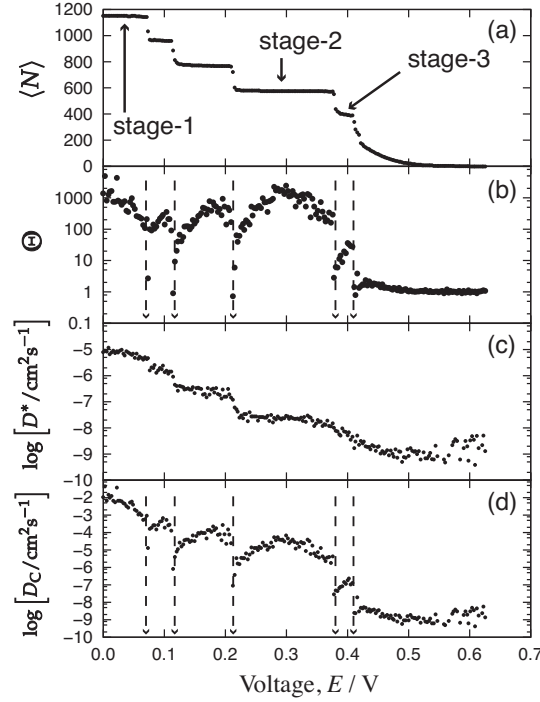
Fig. 7. (a)Number of Li ions in the system, (b)thermodynamic factor, (c)tracer and (d)chemical diffusion coefficients as a function of the applied voltage. We put the origin of the voltage arbitrarily and it is not the standard electrode potential (Li$^+$/Li). The arrows in (b) and (d) mean that Θ and thus D_C should be zero value at those voltages from their definitions.

Figs. 7(c) and 7(d).

It should be noted that phase transition phenomena are usually dependent on their system sizes. We have computed the change of number of Li ions as a function of the applied voltage in three cases of different system sizes, $(n_x, n_y, n_z) = (24, 12, 6)$, $(30, 15, 6)$, and $(42, 20, 6)$. As shown in Fig. 8, there is no difference in the occupancy of Li sites between different sizes except the voltage of change from stage-II to substage. In a large system size, $(42, 20)$, the voltage of change from stage-II to substage is higher than those in smaller systems. The reason for the difference is not clear and the further study would be necessary to clarify the
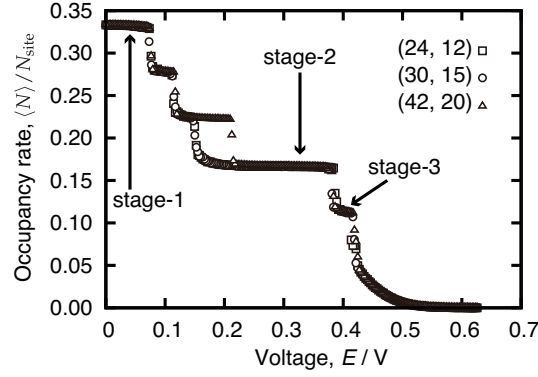
Fig. 8. Occupancy rate of Li sites as a function of the applied voltage with regarding to different system sizes. We can see clear stage separation in all system sizes, but the voltage at which the staging changes from stage-II to substage is not the same between different system sizes.

issue.

4. Concluding Remarks

We have performed Monte Carlo simulation of Li migration in AA-stacking graphite with the effective potential including the interaction between Li ions through host-material deformation. The contributions through the deformation to the Li-Li effective potential were parametrized by the bottom-up procedure using density function theory and molecular statics with classical interatomic potentials which consisted of the repulsive Coulombic interaction, attractive deformation effects between Li ions in the same layer, and the repulsive deformation effects between Li ions of the different layers. Investigations about the deformation effects on Li structures and diffusion coefficients have led us to the following conclusions:

- The $\sqrt{3} \times \sqrt{3}$ super lattice structure in a layer is attributed to the balance between the repulsive Coulombic interaction and attractive deformation effects in the same layer. And

because of the repulsive interaction, the Li diffusivity rises orders of magnitude when the Li density, x in Li_xC_6, becomes close to 1.

- Taking into account the deformation effects between Li ions of different layers, stage structures (stage-1, -2, and -3) are reproduced. The tracer diffusion coefficient moderately increases as Li ion density increases except at $x = 0.5$ and 1.0 where the coefficient jumps orders of magnitude.

- Since the thermodynamic factor drops at the voltages where two stage structures coexist, the chemical diffusion coefficient also drops at the voltages.

- There are some substages found between stage-1 and -2, which some of empty layers of stage-2 are filled with Li ions. Because of the existence of these substages, there are several phase transitions between stage-1 and -2. This may cause further uncertainty in the experimental observation of the chemical diffusion coefficient.

Note that the deformation effects in the on-site potential energy are two-body interactions and thus neglect the many-body screening effect which is important especially in the case of high density situation. Therefore the model potential used in this paper overestimates the deformation effects at high Li density range and the rise of the Li ion diffusivity as a function of Li density would be more gradual if the screening effect is correctly taken into account. So further investigation with the consideration of screening effects would be necessary to discuss quantitatively the change of chemical diffusion coefficient.

References

1) N. Takami, A. Satoh, M. Hara, and T. Ohsaki: Journal of The Electrochemical Society **142** (1995) 371.

2) M. D. Levi and D. Aurbach: Journal of Physical Chemistry B **101** (1997) 4641.

3) A. Funabiki, M. Inaba, and Z. Ogumi: Journal of Electrochemical Society **145** (1998) 172.

4) P. Yu, B. N. Popov, J. A. Ritter, and R. E. White: J. Electrochem. Soc. **146** (1999) 8.

5) H. Yang, H. J. Bang, and J. Prakash: Journal of The Electrochemical Society **151** (2004) A1247.

6) S. A. Safran and D. R. Hamann: Phys. Rev. Lett. **42** (1979) 1410.

7) K. C. Woo, W. A. Kamitakahara, D. P. DiVincezo, D. S. Robinson, H. Mertwoy, J. W. Milliken, and J. E. Fischer: Phys. Rev. Lett. **50** (1983) 182.

8) M. S. Dresselhaus and G. Dresselhaus: Advances in Physics **51** (2002) 1.

9) W. Weppner and R. A. Huggins: Annual Reviews of Materials Science **8** (1978) 269.

10) K. Toyoura, Y. Koyama, A. Kuwabara, F. Oba, and I. Tanaka: Phys. Rev. B **78** (2008) 214303.

11) K. Toyoura, Y. Koyama, A. Kuwabara, and I. Tanaka: Journal of Physical Chemistry C **114** (2010) 2375.

12) K. Persson, Y. Hinuma, Y. Meng, A. V. D. Ven, and G. Ceder: Phys. Rev. B **82** (2010) 125416.

13) K. Persson, V. A. Sethuraman, L. J. Hardwick, Y. Hinuma, Y. S. Meng, A. V. D. Ven, V. Srinivasan, R. Kostecki, and G. Ceder: J. Phys. Chem. Lett. **1** (2010) 1176.

14) N. Ohba, S. Ogata, T. Tamura, S. Yamakawa, and R. Asahi: Computer Modeling in Engineering and Sciences **75** (2011) 247.

15) N. Ohba, S. Ogata, T. Tamura, R. Kobayashi, S. Yamakawa, and R. Asahi: Journal of the Physical Society of Japan **81** (2012) 023601.

16) A. Márquez and P. B. Balbuena: Journal of The Electrochemical Society **148** (2001) A624.

17) J. Yamauchi, M. Tsukada, S. Watanabe, and O. Sugino: Physical Review B **54** (1996) 5586.

18) J. P. Perdow, K. Burke, and M. Ernzerhof: Physical Review Letters **77** (1996) 3865.

19) D. W. Brenner: Phys. Rev. B **42** (1990) 9458.

20) R. Gomer: Reports on Progress in Physics **53** (1990) 917.

21) A. V. D. Ven, G. Ceder, M. Asta, and P. Tepesch: Phys. Rev. B **64** (2001) 184307.

22) A. V. D. Ven, J. Thomas, Q. Xu, B. Swoboda, and D. Morgan: Phys. Rev. B **78** (2008) 104306.

23) J. Backholm, P. Georén, and G. A. Niklasson: Journal of Applied Physics **103** (2008) 023702.